Saturable Inductors For Superior Reflexive Field Containment in Inductive Power Transfer Systems

Alireza Dayerizadeh, Srdjan Lukic
Department of Electrical and Computer Engineering
North Carolina State University
Raleigh, NC, USA
adayeri@ncsu.edu, smlukic@ncsu.edu

***Abstract*—Inductive power transfer has many applications that range from electric vehicle charging to robotics. In dynamic applications, it is required that the segmented transmitter coil transfer power to a moving receiver coil. One proposed method to achieve this is using the reflexive field containment approach presented in the literature. In this work, we improve on the concept by adding a saturable inductor to the system to maximize the difference between the coupled and uncoupled currents in the transmitter coil.**

***Index Terms*—Inductive Power Transfer, Wireless Power Transfer**

NOMENCLATURE

A	Cross sectional area of saturable inductor.
B_{sat}	Saturable inductor core saturation flux density.
C_1 C_2	Secondary side compensation capacitors.
C_{s1}	Primary side series compensation capacitance.
C	Resonant capacitance.
C_{comp}	Primary side parallel compensation capacitance.
C_F	Bandpass filter capacitor.
G	System current gain.
I_{sat}	Saturable inductor saturation current.
I_{peak}	Peak value of AC current through saturable inductor.
$I_{t,uncoupled}$	Transmitting segment uncoupled current.
$I_{t,coupled}$	Transmitting segment coupled current.
k	Coupling factor.
L_2	Secondary side inductance.
L_{s1}	Primary side inductance.
L_F	Bandpass filter inductance.
L_{max}	Saturable inductor inductance value when unsaturated.
L_{eff}	Effective inductance seen by the circuit during saturation.
l_m	Saturable inductor magnetic path length.
M	Mutual inductance.
n	Capacitor "tapping coefficient".
N	Saturable inductor turns.
N_{total}	Total number of transmitting coil segments.
Q	Quality factor of parallel compensated receiver.
R_{eq}	Equivalent load of receiver.
R_r	Real load as seen by primary side in the fully coupled condition.
R_{load}	Load Resistance.
V_{in}	System input voltage.
$Z_{reflected}$	Impedance reflected on to the transmitting coil.
$Z_{t,uncoupled}$	Transmitting segment uncoupled impedance.
$Z_{t,coupled}$	Transmitting segment coupled impedance.
μ	Saturable inductor core permeability.
μ_0	Permeability of free space.
ω	Operating frequency.

I. INTRODUCTION

With the proliferation of electric vehicles and mobile electronic devices, there has been an increased interest in magnetically coupled inductive power transfer (IPT) systems. Numerous low and high power systems that utilize a variety of topology types have proven that IPT efficiencies greater than 90 percent can be achieved [1]. Furthermore, recent studies have demonstrated the feasibility of dynamically charging electric vehicles on the roadway. This approach offers numerous benefits which include increased range and decreased size of on-board energy storage systems [2]-[3]. In consumer electronics, IPT technology has led the push to charge devices, such as smart phones and tablets, with charging pads [4].

However, a significant concern of this technology, particularly in high power applications, is the presence of electromagnetic fields emanating from the system. The International Commission on Non-Ionizing Radiation Protection (ICNIRP) has declared that exposure to time-varying magnetic fields may cause stimulation of nerve and muscle tissue, and the induction of retinal phosphenes [5]. Furthermore, many industry standards, such as the Society of Automotive Engineers (SAE) J2954, set limits for stray electromagnetic fields [6]. Therefore, the control and reduction of stray electromagnetic fields must be addressed if IPT technology is to achieve mass adoption.

Several studies have attempted to address this issue through sensor and power electronics based approaches that require significant additional hardware. One approach involves the control of the coil winding current's phase. The MOSFETs constituting the inverter and active rectifier are duly controlled to control the voltage and current magnitude and phase. This technique was shown to reduce the stray magnetic fields by 30 percent [7]. Another method involves utilizing a resonant reactive shielding coil. The technique employs an additional coil, known as a "shielding coil," with matching capacitors

978-1-5386-1180-7/18/$31.00 ©2018 IEEE

to absorb the leakage magnetic field generated by the IPT transmitting and receiving coils. Since the phase of the current in the shielding coil is opposite to the current in the IPT system, the resulting magnetic fields cancel and reduce the total leakage magnetic field [8]. In [9], a design method for active cancelling of stray electromagnetic fields by way of adding canceling windings to primary and secondary coils is demonstrated.

Recently, a reflexive method utilizing a novel compensation technique has been published [10]. This IPT topology achieves reflexive magnetic field containment through exploiting the receiving coils reflected reactance by utilizing a series compensated LC transmitter with a series-parallel LCC compensated receiver. The result of this technique is that the transmitting coil's current is greatly attenuated when the coils are uncoupled with a corresponding reduction in electromagnetic fields. This compensation technique also allows for one inverter to be connected to multiple LC compensated transmitting coil segments. The magnetic field formed by the transmitter coil can be limited by the position of the receiver without extra control effort or additional hardware.

Building upon these findings, this study introduces a saturable inductor in series with the transmitting coil to enhance the capability in attenuating the current and electromagnetic field strength in the uncoupled condition. The saturable inductor is designed to initiate saturation as the coil's coupling increases, with a corresponding reduction in it's inductive reactance brought upon by the effects of increasing saturation.

II. Reflexive Field Containment: Overview

As mentioned previously, recent work [10] has demonstrated a highly efficient dynamic IPT system that utilizes segmented series compensated LC transmitters with a series-parallel LCC compensated receiver to achieve reflexive field containment. A key feature of this system is the use of a single inverter to power the segmented transmitting coils, as shown in Fig. 1.

A. Receiver Design

In [10], the receiver is designed such that the reflected reactance of the receiver neutralizes the inductive reactance of the transmitter in coupled the condition, resulting in a purely resisitive load seen by the transmitter. The receiver's LCC compensation topology consists of capacitors C_1 and C_2. The variable n, is designated as the *tapping coefficient* and represents the pseudo tapping of the parallel compensation capacitor. The compensation capacitors C_1 and C_2 form a resonant tank at the operating frequency where:

$$C_1 = \frac{n}{n-1} \cdot C \quad C_2 = n \cdot C \tag{1}$$

The relationship between the capacitive and inductive reactances in the receiver is defined by:

$$\omega L_2 - \frac{1}{\omega C_1} = \frac{1}{\omega C_2} \tag{2}$$

where the resonant frequency of the receiver is:

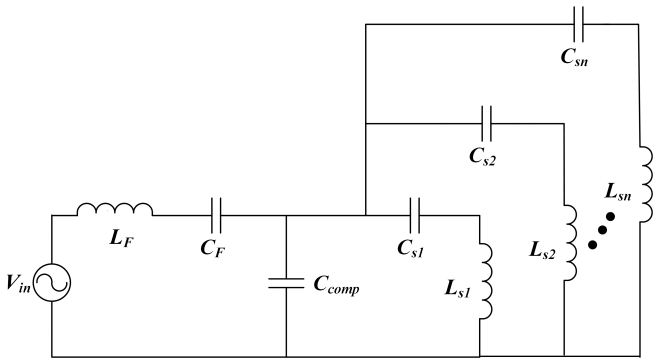

Fig. 1. Primary side topology showing multiple series compensated transmitter coils connected in parallel.

$$\omega = \frac{1}{\sqrt{L_2 C}} \tag{3}$$

Based on analysis detailed in [10], the quality factor of the parallel compensated receiver is denoted by:

$$Q = \frac{R_{eq}}{\omega L_2} \tag{4}$$

The impedance reflected on to the transmitting coil is:

$$Z_{reflected} = \frac{\omega M^2}{L_2}(Q \cdot n^2 - n \cdot j) \tag{5}$$

where M is the constant mutual inductance and is determined prior to designing the system.

B. Transmitter Design

As shown in Fig. 1, the primary side consists of an inverter, represented by voltage source V_{in}, with a bandpass filter formed by L_F and C_F, a parallel compensation capacitor C_{comp}, and multiple series compensated transmitter coils connected in parallel. Each transmitting segment's impedance, when the system is uncoupled, is dominated by the reactive components C_{s1} and L_{s1} [10].

$$Z_{t,uncoupled} = j\omega L_{s1} + \frac{1}{j\omega C_{s1}} \tag{6}$$

The capacitance value of C_{comp} is derived using (6) and N_{total}.

$$C_{comp} = \frac{N_{total}}{\omega Z_{t,uncoupled}} \tag{7}$$

By (5), when the system is in the perfectly coupled condition, the reflected reactance of the receiving coil neutralizes the reactive components present in the transmitting coil, making the resulting impedance purely resistive:

$$\begin{aligned} Z_{t,coupled} &= j\omega L_{s1} + \frac{1}{j\omega C_{s1}} + Z_{reflected} \\ &= \frac{\omega M^2}{L_2} \cdot Q \cdot n^2 = R_r \end{aligned} \tag{8}$$

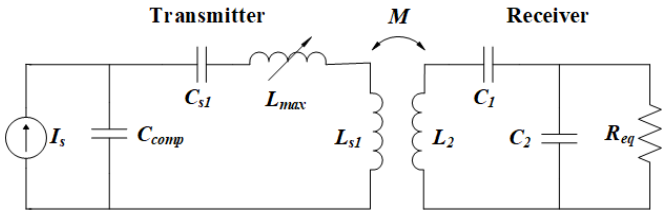

Fig. 2. Proposed topology shown. An inverter with LC band pass filter is represented by current source I_s.

Based on (6) and (8), the current in the transmitter coil in the coupled and uncoupled conditions is represented by:

$$I_{t,uncoupled} = \frac{V_{in}}{Z_{t,uncoupled}} = \frac{V_{in}}{j\omega L_{s1} + \frac{1}{j\omega C_{s1}}} \tag{9}$$

$$I_{t,coupled} = \frac{V_{in}}{Z_{t,coupled}} = \frac{V_{in}}{R_r} \tag{10}$$

where V_{in} is the voltage across C_{comp}. A figure of merit for characterizing the performance of this system topology is the current gain, which is the ratio of the coupled current to the uncoupled current present in the transmitting coil during operation [10].

$$G = \frac{I_{t:coupled}}{I_{t:uncoupled}} = \frac{1}{Q \cdot n} \tag{11}$$

By Ampere's Law, the presence of current in the transmitting coil relates to the presence of emanated electromagnetic fields. Therefore, the value of current gain G indicates the system's overall capability in reflexively containing these emanated electromagnetic fields.

III. Proposed Topology and Operation

The proposed topology, shown in Fig. 2, is a modification of the previously mentioned LC/LCC design. For simplicity, this analysis focuses on a single transmitting segment and receiver. The saturable inductor, L_{max}, is introduced in series with the transmitting coil to increase the overall reactance present in the transmitter circuit when it is unsaturated and the system is uncoupled. This added reactance reduces the current flow in the transmitting coil during this state. Between the uncoupled and fully coupled condition, the saturable inductor commences to saturate as the current in the transmitting coil increases due to the increasing presence of the reflected impedance brought upon by the increase in coupling the coils experience as they become aligned.

A. Saturable Inductor Modeling

When the current through the saturable inductor is less than it's saturation current, the inductor operates in the linear region and it's inductance is equivalent to L_{max}:

$$L_{max} = \frac{\mu\mu_0 N^2 A}{l_m} \tag{12}$$

In a high current case, where saturation has initiated, the saturable inductor's inductance is represented by L_{eff} [11]:

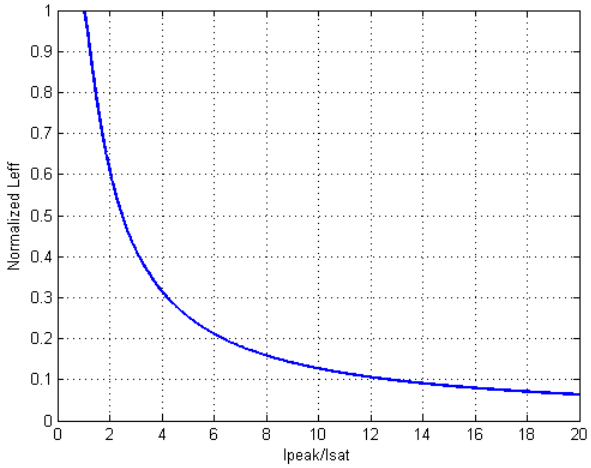

Fig. 3. Effective inductance of the saturable inductor versus current, based on equation (13).

$$L_{eff} = \frac{2L_{max}}{\pi}\left(sin^{-1}(\frac{I_{sat}}{I_{peak}}) + \frac{I_{sat}}{I_{peak}}\sqrt{1-(\frac{I_{sat}}{I_{peak}})^2}\right) \tag{13}$$

$$I_{sat} = \frac{B_{sat} l_m}{\mu\mu_0 N} \tag{14}$$

From (13), it is shown that as the current increases, the effective inductance L_{eff}, decreases as in Fig. 3. For $\frac{I_{peak}}{I_{sat}} > 3$, (13) can be simplified to:

$$L_{eff} = \frac{4L_{max}}{\pi}\left(sin^{-1}(\frac{I_{sat}}{I_{peak}})\right) \tag{15}$$

and by noting $\frac{I_{peak}}{I_{sat}} = \frac{I_{coupled}}{I_{uncoupled}} = G$, we have:

$$L_{eff} = \frac{4L_{max}}{\pi}\left(sin^{-1}(\frac{1}{G})\right) \tag{16}$$

Using (12) and (16), the equivalent inductance of the saturable inductor, in unsaturated and saturated cases can be expressed as:

$$\begin{cases} L_{eff} = L_{max}, & \text{if } I_{sat} > I_{peak} \\ L_{eff} = \frac{4L_{max}}{\pi}\left(sin^{-1}(\frac{1}{G})\right), & \text{if } I_{sat} \leq I_{peak} \end{cases} \tag{17}$$

B. System redesign with saturable inductor

With the introduction of the saturable inductor to the primary side transmitter circuit, the derivation of coupled and uncoupled currents in the transmitter circuit expressed in (9) and (10) respectively, must be reevaluated. When the transmitter and receiver are coupled, the impedance of the transmitter branch with the presence of the saturable inductance is:

$$Z_{t,coupled} = j\omega L_{s1} + j\omega L_{eff} + \frac{1}{j\omega C_{s1}} + Z_{reflected} \tag{18}$$

$Z_{reflected}$ is zero when the receiving coil is absent, and at its maximum value when the coils are fully coupled. The maximum value of $Z_{reflected}$ is driven by the predetermined design value of the mutual inductance M, which is a function of the coils geometric orientation. Substituting (5) for $Z_{reflected}$ in (18) results in:

$$Z_{t,coupled} = \frac{\omega M^2}{L_2} \cdot Q \cdot n^2 + j\left(\omega L_{s1} + \omega L_{eff} - \frac{1}{\omega C_{s1}} - \frac{\omega M^2}{L_2} \cdot n\right) \quad (19)$$

Equating the imaginary part of (19) to zero, the equation for the design of receiver coil is derived as:

$$\frac{\omega M^2}{L_2} \cdot n = \omega L_{s1} + \omega L_{eff} - \frac{1}{\omega C_{s1}} \quad (20)$$

and $Z_{t,coupled}$ becomes resistive:

$$Z_{t,coupled} = \frac{\omega M^2}{L_2} \cdot Q \cdot n^2 \quad (21)$$

Since the value of L_{eff} is known from (16), C_{s1} may be calculated using (20). When the receiver is uncoupled, the impedance of the transmitter branch is:

$$Z_{t,uncoupled} = j\omega L_{s1} + j\omega L_{max} + \frac{1}{j\omega C_{s1}} \quad (22)$$

The values for $I_{t:coupled}$ and $I_{t:uncoupled}$ can be determined based on the inverter input voltage V_{in} and the coupled and uncoupled impendances defined in (21) and (22).

$$I_{t,coupled} = \frac{V_{in}}{Z_{t,coupled}} = \frac{V_{in}}{\frac{\omega M^2}{L_2} \cdot Q \cdot n^2} \quad (23)$$

$$I_{t,uncoupled} = \frac{V_{in}}{Z_{t,uncoupled}} = \frac{V_{in}}{j\omega L_{s1} + j\omega L_{max} + \frac{1}{j\omega C_{s1}}} \quad (24)$$

Therefore, utilizing a saturable inductor value of L_{max}, additional inductive reactance is introduced in the uncoupled condition (24), which maximizes the difference between the coupled and uncoupled currents in the transmitting coil, thereby attenuating the enamanted magnetic fields in the uncoupled condition.

IV. System Design Considerations

From (17), it is noted that for the saturable inductor's performance to be optimum within the circuit, the value of I_{sat} must be greater than I_{peak} when the coils are uncoupled. This condition allows for L_{eff} to equal L_{max} and thus provide the highest possible inductive reactance to attenuate the source coil current in the uncoupled condition. If I_{peak} is greater than I_{sat}, the inductor will experience an initial saturation when the coils are uncoupled thereby reducing it's reactance and diminishing current gain performance.

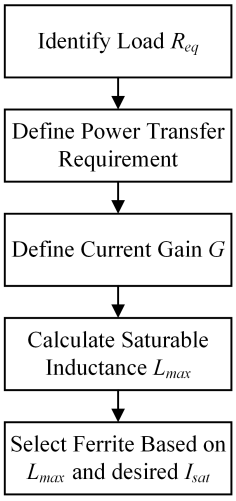

Fig. 4. Flowchart depicting system design process and component selection.

A. Design Process Detail

The design process for the system involves first defining the equivalent real load, R_{eq} to which power is being delivered to by the receiving coil. Per (4), the reciever's quality factor Q, which is a function of R_{eq}, may then be calculated. Following this, using the specified input voltage V_{in}, tapping coefficient n, coupling factor k, and source coil inductance L_{s1}, the total power transferred is determined using (25) as defined in [10].

$$P = \frac{V_{in}^2}{n^2 + (k^2 Q n^2)^2} \frac{k^2 Q n^2}{\omega L_{s1}} \quad (25)$$

The system current gain G and the inductance of the saturable inductor L_{max}, is then defined to meet the desired performance. Once the core material is selected, (12) is used to calculate the designated size and number of turns N required to provide the calculated inductance value. It should again be noted that the resulting L_{eff} calculated using (16) and the chosen C_{s1} must be in adherence to (20). A flow chart (Fig. 4) has been compiled to detail the system design process.

B. Saturable Inductor Considerations

Based on (14), I_{sat} is dependent on the ferrite material properties of saturation flux density B_{sat} and relative permeability μ. Since I_{sat} must be greater than $I_{t,uncoupled}$ and considering (24), it can be deduced that the input voltage V_{in} must also be considered when selecting the appropriate ferrite material. Materials with larger values of B_{sat} allow for higher system input voltage values while not compromising the value of L_{max} by keeping the number of turns N constant. By extension, this allows for flexibility in attaining the desired current gain performance across a wide range of system output power levels.

V. Hardware Validation

A fully functioning IPT system based on the components listed on Table I, utilizing the LC/LCC compensation technique and saturable inductor, was built and tested (Fig. 5

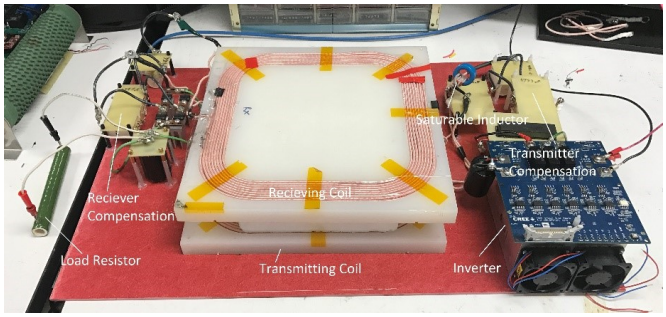

Fig. 5. Hardware validation inductive power transfer setup.

Fig. 6. EPCOS T38 saturable inductor core with N=4 turns.

and 6). For the purposes of this study, only one transmitting segment was tested and the power transfer level was kept at approximately 50W. Utilizing the methodology noted in the previous section, the load, power transfer requirement, and desired current gain was first specified. Following this, the required L_{max} value for the saturable inductor was calculated to be 160uH. An EPCOS T38 core with 4 turns was then selected to give this inductance value while simultaneously providing an I_{sat} value of approximately .5 Amperes to allow for the required V_{in} of 20 volts.

Using a Tektronix TCP0030A current probe and Tektronix P5200A differential voltage probe, the current through the transmitting coil and the voltage across C_{comp}, was measured in both uncoupled and coupled conditions and shown in Fig. 7 and 8. The phase difference of the current and voltage waveform can be seen in both coupling conditions for the transmitting coil. This phase shift is indicative of the presence of the large inductive reactance in the uncoupled condition. During operation, the RMS of the current waveforms through the transmitting coil corresponding to $I_{t:uncoupled}$ and $I_{t:coupled}$, were measured to be .398 Amperes and 4.06 Amperes respectively. The observed current gain G is thus approximately 10.2.

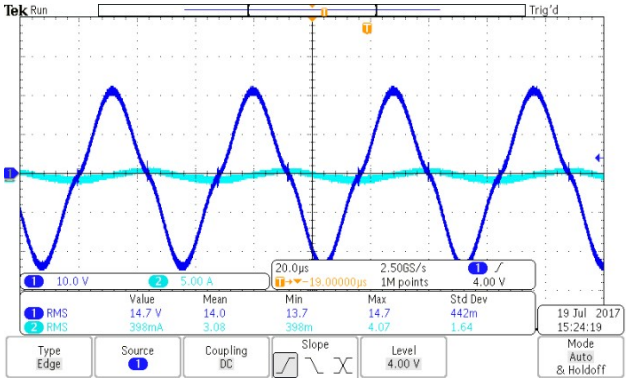

Fig. 7. Current (cyan) and voltage (blue) wave forms shown for the uncoupled condition.

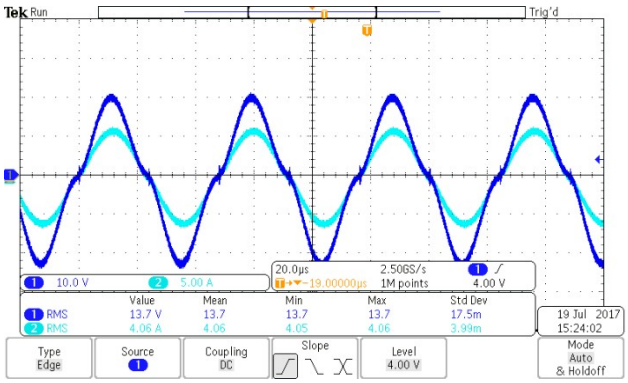

Fig. 8. Current (cyan) and voltage (blue) wave forms shown for the fully coupled condition.

TABLE I

IPT system component values, designed for 22 KHz operating frequency, used for hardware validation.

Segment	Component	Value
Transmitter	L_{s1}	$191uH$
	L_{max}	$160uH$
	L_{eff}	$10uH$
	C_{s1}	$430nF$
	C_{comp}	$755nF$
Receiver	L_2	$191uH$
	C_1	$330nF$
	C_2	$1616nF$
	R_{Load}	1.1Ω

VI. Conclusion

It has been demonstrated that through the use of a saturable inductor, a high level of current attenuation can be achieved when the system is uncoupled that correspondingly reduces the induced electromagnetic field emissions. The overall current gain G, demonstrated (10.2) by this system is over double the performance achieved by the reflexive field containment system configuration in previously reported findings [10]. The technique detailed in this study may be scaled and applied to a wide variety of applications where electromagnetic field emissions are of concern, such as electric vehicle charging, industrial or consumer electronic applications.

References

[1] H. H. Wu, A. Gilchrist, K. D. Sealy, and D. Bronson, "A high efficiency 5 kw inductive charger for evs using dual side control," *IEEE Transactions on Industrial Informatics*, vol. 8, no. 3, pp. 585–595, 2012.

[2] C. C. Mi, G. Buja, S. Y. Choi, and C. T. Rim, "Modern advances in wireless power transfer systems for roadway powered electric vehicles," *IEEE Transactions on Industrial Electronics*, vol. 63, no. 10, pp. 6533–6545, 2016.

[3] K. Hata, T. Imura, and Y. Hori, "Dynamic wireless power transfer system for electric vehicles to simplify ground facilities - power control and efficiency maximization on the secondary side," in *2016 IEEE Applied Power Electronics Conference and Exposition (APEC)*. IEEE, 2016, pp. 1731–1736.

[4] S. Y. Hui, "Planar wireless charging technology for portable electronic products and qi," *Proceedings of the IEEE*, vol. 101, no. 6, pp. 1290–1301, June 2013.

[5] "Icnirp guidelines for limiting exposure to time-varying electric, magnetic and electromagnetic fields (1 hz to 100 khz)," *Health Phys.*, vol. 99, pp. 818–836, 2010.

[6] *Wireless Power Transfer for Light Duty Plug-In Electric Vehicles and Alignment Methodology*, no. SAE Standard J2954, 2016.

[7] M. Lu and K. D. T. Ngo, "Attenuation of stray magnetic field in inductive power transfer by controlling phases of windings x2019; currents," *IEEE Transactions on Magnetics*, vol. 53, no. 9, pp. 1–8, Sept 2017.

[8] J. Park, D. Kim, K. Hwang, H. H. Park, S. I. Kwak, J. H. Kwon, and S. Ahn, "A resonant reactive shielding for planar wireless power transfer system in smartphone application," *IEEE Transactions on Electromagnetic Compatibility*, vol. 59, no. 2, pp. 695–703, April 2017.

[9] S. Y. Choi, B. W. Gu, S. W. Lee, W. Y. Lee, J. Huh, and C. T. Rim, "Generalized active emf cancel methods for wireless electric vehicles," *IEEE Transactions on Power Electronics*, vol. 29, no. 11, pp. 5770–5783, Nov 2014.

[10] K. Lee, Z. Pantic, and S. M. Lukic, "Reflexive field containment in dynamic inductive power transfer systems," *IEEE Transactions on power Electronics*, vol. 29, no. 9, pp. 4592–4602, 2014.

[11] S. Chung, S. Huang, J. Huang, and E. Lee, "Applications of describing functions to estimate the performance of nonlinear inductance," *IEE Proceedings-Science, Measurement and Technology*, vol. 148, no. 3, pp. 108–114, 2001.